Phase bubbles and spatiotemporal chaos in granular patterns

Sung Joon Moon,[1,*] M. D. Shattuck,[1,†] C. Bizon,[2] Daniel I. Goldman,[1] J. B. Swift,[1] and Harry L. Swinney,[1,‡]
[1]*Center for Nonlinear Dynamics and Department of Physics, University of Texas, Austin, Texas 78712*
[2]*Colorado Research Associates Division, Northwest Research Associates, Inc., 3380 Mitchell Lane, Boulder, Colorado 80301*
(Received 1 July 2001; published 4 December 2001)

We use inelastic hard sphere molecular dynamics simulations and laboratory experiments to study patterns in vertically oscillated granular layers. The simulations and experiments reveal that *phase bubbles* spontaneously nucleate in the patterns when the container acceleration amplitude exceeds a critical value, about $7g$, where the pattern is approximately hexagonal, oscillating at one-fourth the driving frequency ($f/4$). A phase bubble is a localized region that oscillates with a phase opposite (differing by π) to that of the surrounding pattern; a localized phase shift is often called an *arching* in studies of two-dimensional systems. The simulations show that the formation of phase bubbles is triggered by undulation at the bottom of the layer on a large length scale compared to the wavelength of the pattern. Once formed, a phase bubble shrinks as if it had a surface tension, and disappears in tens to hundreds of cycles. We find that there is an oscillatory momentum transfer across a kink, and the shrinking is caused by a net collisional momentum inward across the boundary enclosing the bubble. At increasing acceleration amplitudes, the patterns evolve into randomly moving labyrinthian kinks (spatiotemporal chaos). We observe in the simulations that $f/3$ and $f/6$ subharmonic patterns emerge as primary instabilities, but that they are unstable to the undulation of the layer. Our experiments confirm the existence of transient $f/3$ and $f/6$ patterns.

DOI: 10.1103/PhysRevE.64.0613XX PACS number(s): 45.70.Qj, 47.54.+r

I. INTRODUCTION

Spatiotemporal chaos, where the physical variables vary in time and space in a seemingly random way, may arise when a spatially extended system is driven far from the primary instability [1]. In some systems, spatiotemporal chaos is understood as a complicated evolution of the amplitude field, and the behavior can be described in terms of the dynamics of this field [2]. In some other systems, the dynamics of defects plays a primary role in the transition to spatiotemporal chaos; cases include Rayleigh-Bénard convection [3,4], electrohydrodynamic convection [5], chemical patterns [6], and Faraday instabilities [7]. Several mathematical models have been proposed to describe the transition to spatiotemporal chaos in spatially extended physical systems, including amplitude chaos [8], phase turbulence [9], defect-mediated turbulence [10,11], and invasive defects [12], but the understanding is still far from complete.

In this paper, we study patterns around the transition from the $f/4$ subharmonic hexagonal pattern to spatiotemporal chaos in granular layers with large aspect ratio ($L/H \gtrsim 10$, where L is the characteristic horizontal size of the layer, and H is the depth of the layer). The layers are subject to a sinusoidal oscillation in the direction of gravity. The oscillation is characterized by two nondimensional control parameters, $\Gamma = 4\pi^2 f^2 A/g$ and $f^* = f\sqrt{H/g}$, where A is the amplitude of the oscillation, $f = 1/T$ is the frequency of the oscillation, T is the period of the oscillation, and g is the acceleration due to gravity. We also define the nondimensional depth of the layer, $N = H/\sigma$, where σ is the diameter of the particle. Various subharmonic standing wave patterns have been observed as a function of Γ and f^* [13]; however, the transition to spatiotemporal chaos has not previously been investigated. In this study, we show that the transition to spatiotemporal chaos in granular patterns is due to the intrinsic dynamics of oscillated granular layers: a large length scale undulation of the layer, and an oscillatory momentum transfer across a kink.

The rest of the paper is organized as follows. Section II presents the methods in the simulation and the experiment. Kinks, phase bubbles, and randomly moving labyrinths are described in Sec. III. In Sec. IV a large length scale undulation of the layer and its relation to the nucleation of a phase bubble is described. Section V discusses how a phase bubble shrinks and disappears. In Sec. VI, the prediction and observation of transient $f/3$ and $f/6$ patterns are presented, and the paper is concluded in Sec. VII.

II. METHODS

A. Numerical simulation

In the absence of well-validated macroscopic governing equations for vertically oscillated granular layers, current theoretical investigation proceeds at a more basic level, that of individual particles. Bizon *et al.* [14] developed an event-driven inelastic hard sphere molecular dynamics simulation of this system, by implementing the collision operators in Ref. [15]. This collision model conserves both linear and angular momentum, but allows energy to be dissipated through inelastic collisions and surface friction. The normal coefficient of restitution $e(v_n)$ depends on the magnitude of the normal component of relative colliding velocity v_n

*Electronic mail: moon@chaos.ph.utexas.edu
†Present address: Department of Physics, City College of CUNY, New York, NY 10031-9198.
‡Electronic mail: swinney@chaos.ph.utexas.edu

$=(\mathbf{v}_1-\mathbf{v}_2)\cdot\hat{\mathbf{r}}_{12}$, where $\hat{\mathbf{r}}_{12}=(\mathbf{r}_1-\mathbf{r}_2)/|\mathbf{r}_1-\mathbf{r}_2|$. The accurate form of $e(v_n)$ is not known; it was assumed that $e(v_n)=1-Bv_n^{3/4}$ for v_n less than a crossover velocity v_c, and $e(v_n)=e_0$ otherwise. The value of B was set to make $e(v_n)$ continuous at $v_n=v_c$. Here we use $v_c=\sqrt{g\sigma}$ and $e_0=0.7$. The simulation results are not sensitive to the form of $e(v_n)$ for $v_n<v_c$. The tangential impulse is given by a coefficient of friction μ times the normal impulse, with a cutoff corresponding to the crossover from a sliding contact to a rolling contact. The crossover ratio of the relative surface velocity after the collision to that of before the collision, $-\beta_c$, was set to -0.35 as suggested in Ref. [15], and μ was set to 0.5. The values of these parameters were chosen to fit the wavelength of the pattern obtained in the experiments with lead particles, for three different control parameter sets. These fitting parameters reproduced the observed patterns quantitatively throughout the control parameter space [14]. The collisions between the grains and the container were treated in the same way as the collisions between grains. The mass of the container was assumed to be infinitely large compared to that of the granular layer.

We performed three types of simulations: (1) two dimensional (2D), (2) quasi-2D, and (3) 3D. We simulated a 2D (Figs. 3 and 10) or quasi-2D layer as vertical cross section of a 3D layer. A quasi-2D layer is a 3D layer whose dimension in one direction is short enough ($\lesssim 10\sigma$) to be homogeneous in that direction; these simulations run much faster than fully 3D simulations, yet yield the same statistical information [Figs. 7, 8, and 11(a)]. We performed simulations of 3D layers of square shape with horizontal periodic boundary condition [Fig. 11(b)] and of 3D layers of cylindrical shape with side wall, when we compare with the experiments (Figs. 4 and 9).

B. Experiment

Experiments were conducted with vertically oscillated layers of granular material consisting of spherical bronze particles of mean diameter 165 μm (spherical lead particles of diameter 165 μm were used only for Fig. 1). The nondimensional depth of the layer, N, was in the range of 5–15, and the aspect ratio L/H ranged from 40 to 150. Both circular and rectangular containers with various sizes were used in the experiments. The container was mounted on an electromagnetic shaker, and it oscillated sinusoidally in the direction of gravity with a single frequency, in the range 10–150 Hz. The value of Γ varied from 0 to 14. The container was evacuated to a pressure of 4 Pa to reduce the role of interstitial gas. The container was encircled by a ring of light-emitting diodes (LED's) and the images were taken by a digital camera mounted above the container. A more detailed description of the experimental apparatus is found in Ref. [16].

III. PATTERNS AROUND A TRANSITION TO SPATIOTEMPORAL CHAOS

The phase diagram of the patterns in oscillated granular layers has been reported previously [13,14,16]. We present a new phase diagram in Fig. 1 that shows the details above the $f/4$ subharmonic hexagonal pattern regime, which is the focus of the current study.

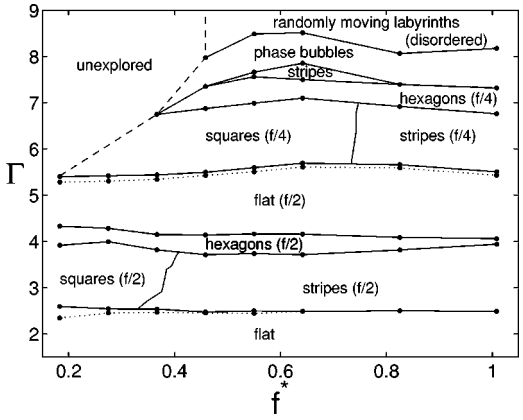

FIG. 1. Phase diagram obtained from an experiment with bronze particles of diameter $\sigma=165\,\mu$m and nondimensional depth $N=5$, in a circular container with diameter $L=770\sigma$, showing particularly the details for $\Gamma>7.0$. Solid lines denote the transitions for increasing Γ, while the dotted lines denote decreasing Γ.

A. Single inelastic ball model and temporal dynamics of the layer

Much of the dynamics of the patterns in this system can be understood from the single inelastic ball model [16,17]. In this section we review the results of this model in the $f/2$ and $f/4$ patterns regime. The single ball model is a one-dimensional model of the oscillated granular layer, which approximates the center of mass of the layer as a completely inelastic ball ($e=0$) on an oscillating plate.

For $\Gamma>1$, the magnitude of the acceleration of the container exceeds g during a fraction of the cycle, so that the layer loses contact with the container when the plate's acceleration becomes $-g$, and then the layer makes a free flight until colliding with the container later. In the $f/2$ square-stripe pattern regime, the flight time of the layer is a fraction of the oscillation period T, and the layer leaves and hits the container every cycle [Fig. 2(a)]. In this regime, the magnitude of the acceleration of the container at the collision is less than g [the ball hits below the dot-dashed line in Fig. 2(a)], and the layer stays on the container until the acceleration becomes $-g$ again (the intersection of the dot-dashed line and the trajectory of the plate). The layer leaves the container at the same phase angle of the oscillation at every cycle; hence the take-off velocity or the flight time is single valued. This regime is called *Period 1*, $n=1$, which means the period of the trajectory is single valued (*Period 1*) and the ball collides with the plate every cycle ($n=1$). For $\Gamma\gtrsim 4.0$, the trajectory consists of two different flight times, and the flight time is still a fraction of the period T [Fig. 2(b), *Period 2*, $n=1$]; it corresponds to the $f/2$ hexagonal pattern. In this regime, the magnitude of the container acceleration at collision is larger than g once every other cycle [the ball hits above the dot-dashed line in Fig. 2(b)]. At this collision, the layer leaves the container immediately, and the take-off ve-

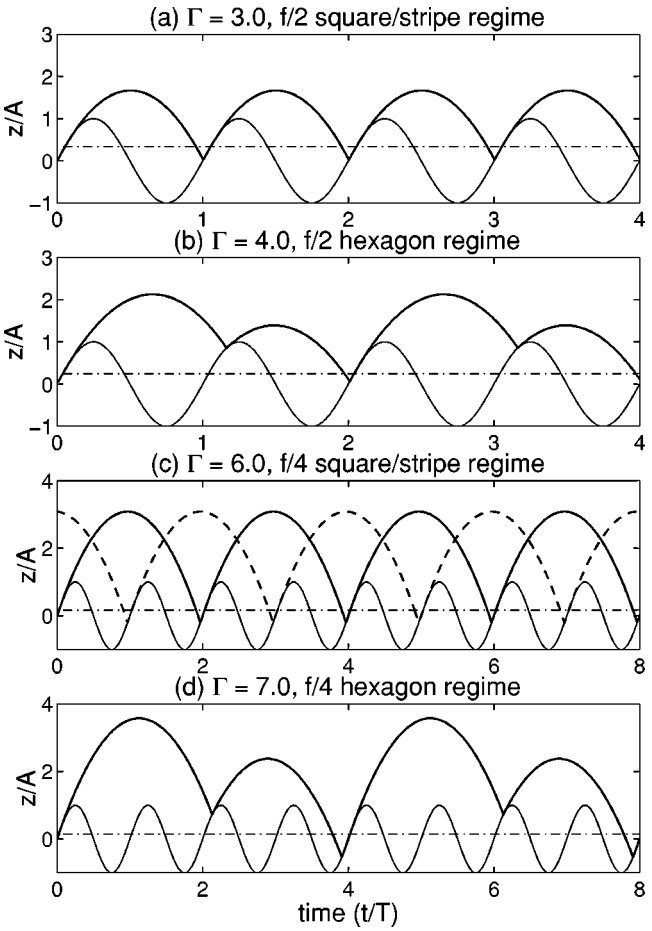

FIG. 2. Temporal trajectory of a completely inelastic ball ($e=0$) on an oscillating plate, which models the trajectory of the center of mass of the layer. The solid sinusoidal curve is the trajectory of the plate. The ball leaves the plate when the acceleration of the plate becomes $-g$; i.e., where the horizontal dot-dashed line intersects with the trajectory of the ball. If the ball collides with the plate above the dot-dashed line [in (b) and (d)] it leaves the plate immediately.

locity and flight time are smaller than those of the other cycles, in which the ball stays on the container until the acceleration of the container becomes $-g$.

For values of Γ above 4.5, the flight time of the layer exceeds T, and the layer hits the container once every other cycle. In this regime, the layer can hit the container either on odd cycles or on even cycles; the trajectory becomes degenerate (the trajectory in the $f/2$ hexagonal pattern regime is also degenerate, and a $f/2$ hexagonal pattern can have a phase discontinuity defect, which is different from a kink). The trajectory of single inelastic ball in the $f/4$ square-stripe pattern regime ($\Gamma \gtrsim 5.5$) is shown in Fig. 2(c) (*Period 1*, $n=2$). When Γ is increased to 6.5, the trajectory of the layer consists of longer and shorter flight times, and a bifurcation to the $f/4$ hexagonal pattern occurs [Fig. 2(d), *Period 2*, $n=2$]. At $\Gamma \sim 8.0$, another bifurcation to *Period 1* and $n=3$ state occurs, which corresponds to a $f/3$ flat pattern; however, the $f/3$ flat pattern has not been observed before, and the layer has been known to exhibit spatiotemporal chaos in this regime. We found transient $f/3$ and $f/6$ patterns in this study (see Sec. VI).

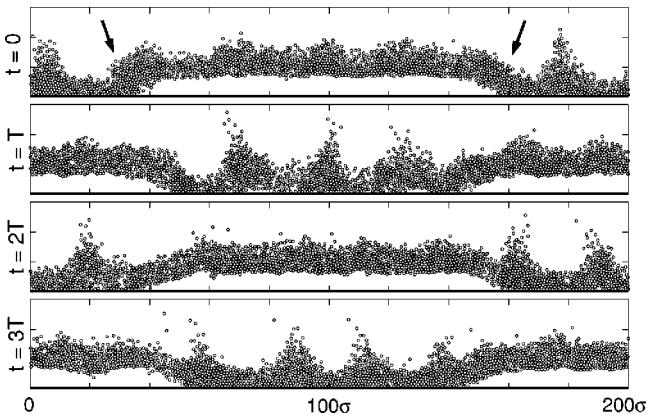

FIG. 3. A side view of a 2D layer of an $f/4$ pattern with two kinks, obtained in the simulation for $\Gamma=6.5$, $f^*=0.8$, and $N=8$. The middle part and the rest of the layer oscillate π out of phase, and phase discontinuities between these two phase domains are called kinks (indicated by arrows). The container (horizontal bar at the bottom) is at its minimum height at the phase angle at which these figures are taken. Horizontal boundary is periodic.

Since the layer collides with the container every other cycle for $\Gamma > 4.5$, domains π out of phase may coexist in the layer. When these opposite phase domains coexist, there is a phase discontinuity line defect between the adjacent phase domains, which we call a kink [16] (two sides of a phase discontinuity defect in the $f/2$ hexagonal pattern regime are not at opposite phases, and this defect is not a kink). In the experiments, kinks are created by inhomogeneous initial conditions or external perturbations such as side wall friction or tilt of the container; see Sec. IV. A sequence of an $f/4$ pattern with kinks obtained from a 2D simulation is shown in Fig. 3, where one domain has fully developed a pattern, and the other is nearly flat (see Ref. [18]).

B. Phase bubbles and randomly moving labyrinths

As Γ is increased further from the $f/4$ hexagonal pattern regime, the layer exhibits spatiotemporal chaos, which is not included in the single ball model. Snapshots obtained from the experiments and simulations of this regime are shown in Fig. 4.

As Γ is increased above a critical value Γ_{pb} in the $f/4$ hexagonal pattern regime, a small localized region spontaneously changes its phase angle, and this region becomes enclosed by a kink. We call this localized region a phase bubble; see Figs. 4(c) and 4(d). Phase bubbles suddenly (in one cycle) pop up at random locations, and they shrink and disappear over several tens to hundreds of cycles. The nucleation rate increases with Γ, and the decay time depends on the control parameters and the initial size. Γ_{pb} varies with the depth of the layer and the material used; it is 7.5 in the experiment with bronze particles and $N=5$, and is 7.1 in layers of lead particles with $N=5$, in three dimensions. In the simulations we find that the value of Γ_{pb} is a few percent

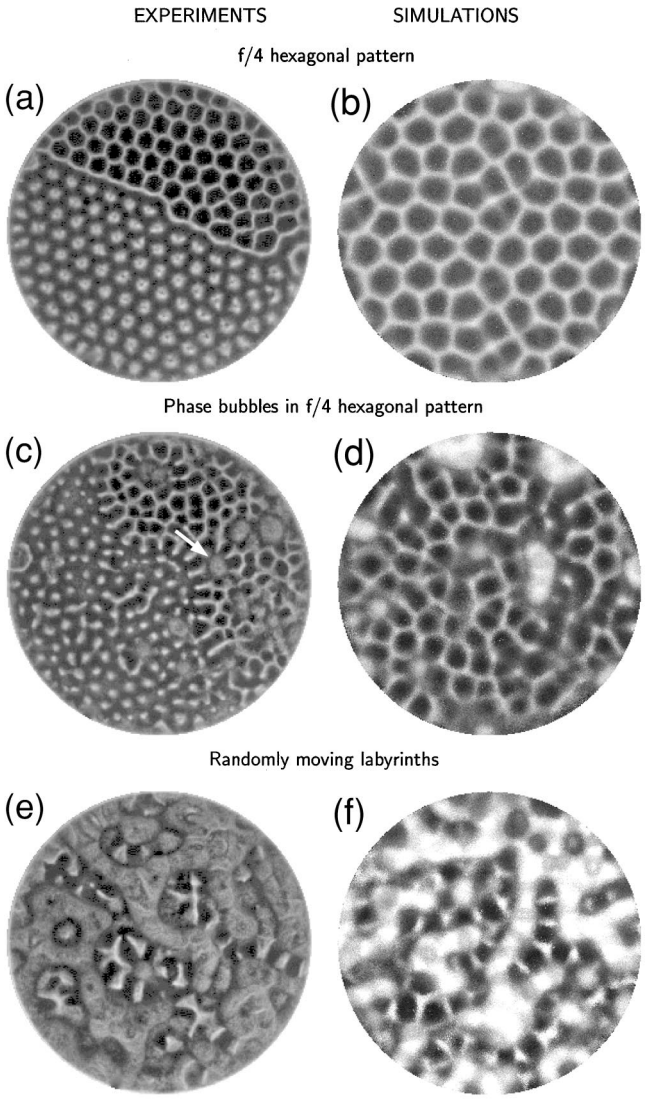

FIG. 4. Top views obtained from the experiments, and the mean height as a function of the position obtained from 3D simulations. In (a) and (c), there is a phase kink near the middle, while there is not in (b) or (d). Kinks are easily created in the experiment due to the side wall friction or tilt of the layer, but they are easily eliminated in the simulation; see Sec. IV. One phase bubble is indicated by a white arrow in (c); in (d) the phase bubbles are the white areas, because they reach their maximum height at this moment and patterns superposed on them are nearly flat. The gray scale in the experimental images indicates the intensity of the reflected light, which is a measure of the gradient of the surface. The gray scale in the simulation images is $\langle z\rangle(x,y)$, increasing from black to white, where $\langle F\rangle(x,y)$ is an averaged value of F over the particles located at (x,y);$\langle z\rangle(x,y)$ is called the mean height field. A circular container of diameter $L=847\sigma$ is used in the experiments, and a circular container of $L=294\sigma$ is simulated. The parameters (Γ, f^*, N) are (a) (7.1, 1.0, 10), (b) (7.0, 0.85, 8), (c) (7.3, 1.0, 10), (d) (7.2, 0.85, 8), (e) (8.0, 1.2, 15), and (f) (8.9, 0.85, 8).

smaller in 2D or quasi-2D layers than in 3D. A phase bubble is not just a defect in the $f/4$ hexagonal pattern of this system; it arises due to an inherent instability of the oscillated granular layer (see Sec. IV). Phase bubbles are spontaneously nucleated even without side wall friction or any other external perturbation, while kinks for $4.5<\Gamma<\Gamma_{pb}$ are never created spontaneously without an external perturbation.

As Γ is further increased, the nucleation rate of phase bubbles increases faster than the decay rate, and the layer eventually exhibits spatiotemporal chaos in the form of randomly moving labyrinths [Figs. 4(e) and 4(f)]. Note that there are a few kinks of closed form; i.e., phase bubbles. In this regime, labyrinthian kinks move around in the container in a seemingly random fashion. Each phase domain of labyrinths collides with the container every other cycle, and an $f/4$ subharmonic pattern is superposed on it. The layer behavior does not show any qualitative difference up to $\Gamma \sim 14$, the highest value investigated in the experiment.

As a phase bubble shrinks, it becomes more circular, as though it had a surface tension. This behavior is more clearly observed with phase bubbles in the $f/2$ flat pattern regime, because there is no superposed pattern. Phase bubbles are not nucleated spontaneously for $\Gamma<\Gamma_{pb}$, but we can make them from initial conditions with inhomogeneous phase, by suddenly decreasing Γ from the randomly moving labyrinths regime to the $f/2$ flat pattern regime. Such phase bubbles in the $f/2$ flat pattern regime are shown in Fig. 5. See Ref. [18].

A kink acts on the pattern as if it were a boundary, and the pattern tries to rotate perpendicular to the kink. These ''boundaries'' of the layer have irregular shape; a well-ordered hexagonal pattern does not form in the phase bubble regime because phase bubbles break the long range order of the pattern [Figs. 4(c) and 4(d)]. Pattern selection is also affected by the size of a phase bubble, or the width of a phase domain in the randomly moving labyrinths regime because of the ''boundary condition'' of the pattern imposed by the kink. When a phase bubble is larger than the wavelength of the hexagonal pattern, the phase bubble has an $f/4$ hexagonal pattern superposed on it. Otherwise, an $f/4$ stripe pattern is superposed because it is the only pattern that can fit in such small domains.

IV. NUCLEATION OF PHASE BUBBLES

We find in the simulation that for Γ slightly below Γ_{pb}, the bottom of the layer exhibits an undulation, of which length scale is much larger than the wavelength of the pattern. In this section, we discuss how the undulation leads to the nucleation of phase bubbles.

In the $f/4$ hexagonal pattern and the phase bubble regime, the temporal dynamics of the layer is sensitive to a small change in the flight time. This is the case also in the single ball model; in the $f/4$ hexagonal pattern regime, the ball immediately leaves the container at every other collision, so that the instantaneous velocity of the container at this collision becomes the take-off velocity of the ball. Thus, if the velocity is changed slightly and the flight time is increased, the take-off velocity at the next flight becomes smaller; this velocity may be too small for the ball to fly over the container during the following two cycles, so that the ball collides with the container in the very next cycle (Fig. 6). In a real layer, the flight time has some fluctuation due to the

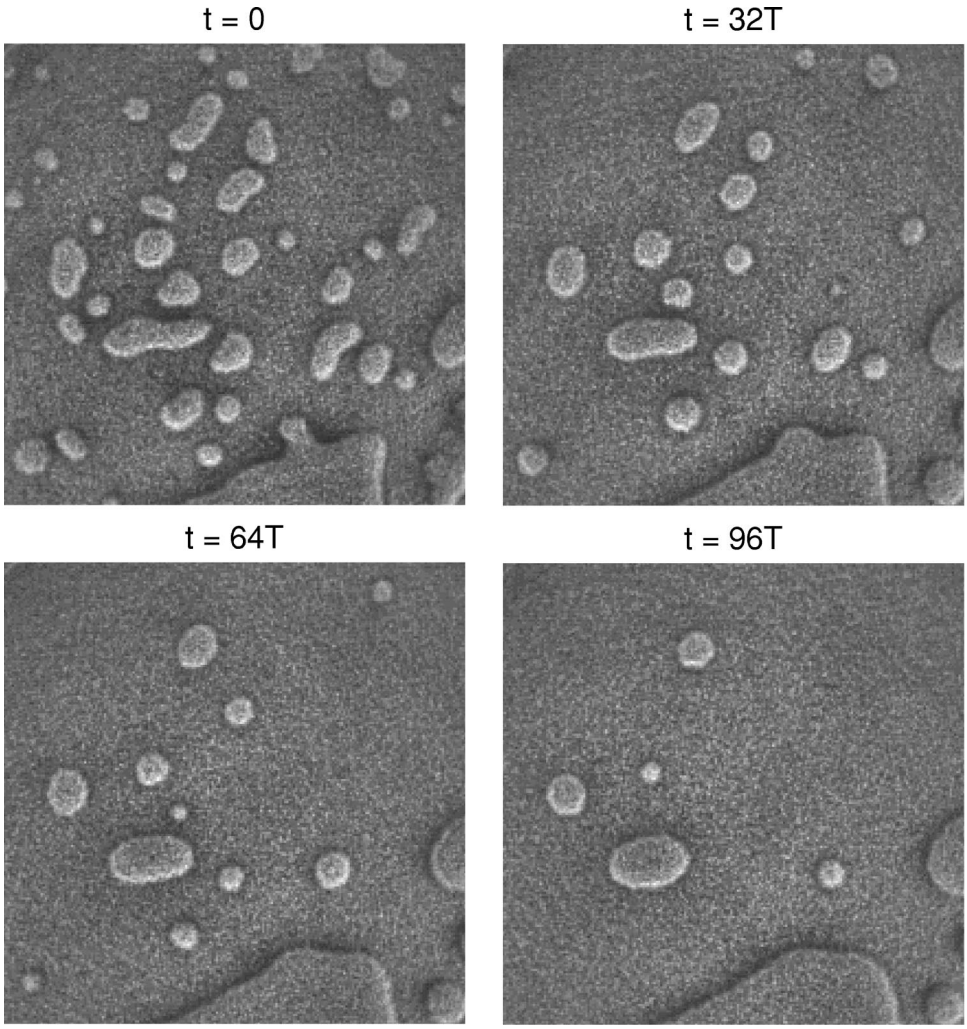

FIG. 5. A sequence of phase bubbles in an $f/2$ flat pattern, obtained in the experiment. The bubbles shrink as if they had a surface tension. To create these phase bubbles, Γ was suddenly decreased from 9.0 to the $f/2$ flat pattern regime, $\Gamma=4.5$ ($f^*=0.6$). Experimental setup is the same as in Fig. 1. $400\sigma\times400\sigma$ portion of the layer is shown.

undulation; the mechanism in Fig. 6 will create a phase bubble when the undulation is big enough (Fig. 7).

The power spectral densities (PSD's) of the top and the bottom of a layer for values of Γ slightly below Γ_{pb} show that another peak with small wave numbers appears as Γ approaches Γ_{pb} (Fig. 8). For smaller Γ ($\Gamma\lesssim6.5$ for this case), the shape of the bottom of the layer is slaved to the top of the layer and has the same wavelength as the top; PSD's have peaks only at the wavelength of the pattern and its subharmonics.

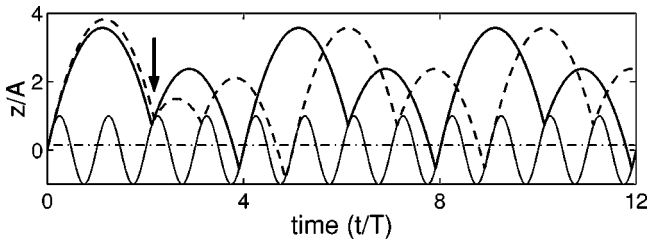

FIG. 6. Sensitivity of the trajectory to small perturbations is illustrated by perturbed (dashed line) and unperturbed (solid line) trajectories of a completely inelastic ball in the $f/4$ hexagonal pattern regime ($\Gamma=7.0$). For the perturbed trajectory, we increased the initial take-off velocity by 3% to delay the collision. At the next collision (indicated by an arrow), the perturbed ball collided with the container because its take-off velocity was too small, and its trajectory became out of phase with that of unperturbed one.

The nucleation rate of phase bubbles monotonically increases with Γ; we hypothesize that the amplitude or the growth rate of the undulation increases with Γ. Above some value of Γ ($>\Gamma_{pb}$), the nucleation rate exceeds the decay rate, and phase bubbles or kinks accumulate in the layer until each phase domain reaches the shortest length scale that cannot have another kink in it; i.e., this sets the width of the labyrinths. As a result, the layer is filled with a superposition of phase bubbles that connect to one another, forming nonclosed kinks. We propose that the randomly moving labyrinth pattern results from the above mechanism, i.e., randomly moving labyrinths may be understood as a ''saturated'' state of phase bubbles.

There are two more mechanisms responsible for the creation of phase bubbles or kinks: (1) side wall friction and (2) tilt of the layer. In an infinitely extended layer without side walls, kinks are formed only by the undulation of the layer, or nucleation of phase bubbles, if the layer is perfectly level. In the simulation, side walls are easily eliminated by imposing horizontal periodic boundary conditions; however, the layer size is always finite in the experiment, and the side wall

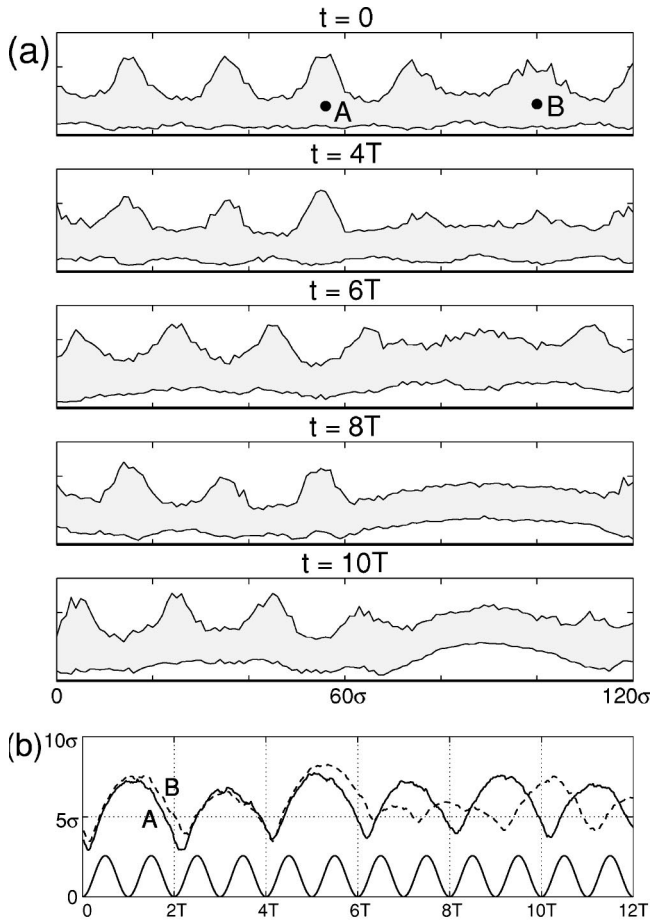

FIG. 7. (a) A sequence of side views of a quasi-2D layer showing the nucleation of a phase bubble around **B**, obtained in a simulation of a quasi-2D layer of size $200\sigma\times10\sigma$, for $\Gamma=7.2$, $f^*=0.9$, and $N=6$. (b) The trajectories of the center of mass at two horizontal locations, **A** and **B** in (a) as a function of time. The sinusoidal function shown in (b) is the trajectory of the plate of the container. At $t=0$ in (a), the bottom of the layer has a short length scale deformation slaved to the pattern on the surface of the layer. This undulation at the bottom grows, as shown in the next two successive frames in (a) [$t=4T$ and $6T$ in (b)]. At $t=6T$, the collision of **B** is delayed due to the undulation; at this collision, a portion of the layer around **B** collides with the container when the plate nearly reaches its maximum height, and the take-off velocity becomes too small to fly the next two cycles over the container. As a result, **B** collides with the container at the very next cycle, at $t\sim7T$, and it becomes nearly π out of phase with the rest of the layer. This mechanism is the same as that in Fig. 6.

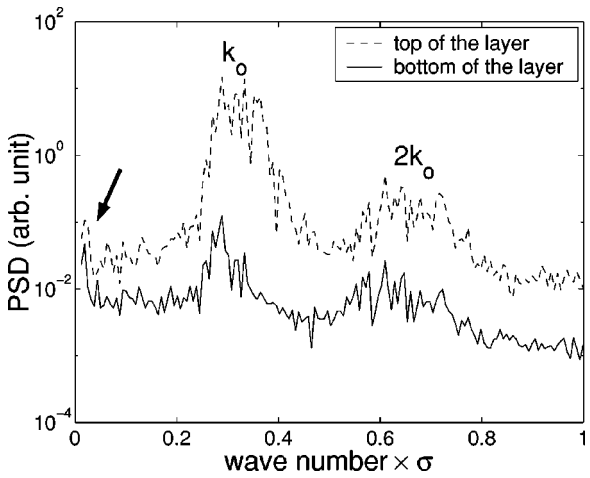

FIG. 8. Power spectral densities (PSD's) of the top and the bottom of a quasi-2D layer for $\Gamma=6.6$, $f^*=0.9$, and $N=6$, obtained in simulations of a quasi-2D layer of size $1000\sigma\times10\sigma$ having more than 50 wavelengths; there is an additional peak (indicated by an arrow) at a small wave number, as well as the primary peaks at the wave number of the pattern (at $k_0=2\pi\sigma/\lambda$, where λ is the wavelength of the pattern) and at $2k_0$. $\Gamma_{pb}=6.7$ for this simulation. PSD's were determined when the amplitude of the pattern was fully developed, just before the layer collided with the container.

effect cannot be completely eliminated. In the experiment, the friction due to the side walls disturbs the oscillatory motion of the layer, which often creates kinks. This effect becomes more and more important as Γ is increased. There are some phase bubbles in contact with the side wall in Figs. 4(c) and 4(d), which are kinks created by the side wall friction. In the randomly moving labyrinths regime, the side wall effect is one of the major reasons for the decay of $f/3$ or $f/6$ transient patterns (see Sec. VI). In addition to the above effect, tilt of the container also creates kinks. This is the main mechanism of the creation of kinks for $4.5<\Gamma<\Gamma_{pb}$ in the experiment.

V. DYNAMICS OF A PHASE BUBBLE

Once formed, a phase bubble shrinks as if it had a surface tension, and then disappears (Fig. 5). We now discuss why this happens.

When the layer collides with the plate, a density wave forms and propagates across the boundary of a phase bubble (a kink). This density wave initiates a collisional momentum transfer in the horizontal as well as in the vertical direction, across a kink (Fig. 9). A sequence of side views of a kink in a 2D layer is in Fig. 10, which shows the relation for the density wave to the momentum transfer. At $t=0$ in Fig. 10, the left half of the layer collides with the plate (horizontal bar) and is pushed up. It becomes compact and nearly static with respect to the plate, acting as if it were a part of the container. At this moment, the rest of the layer is still falling and is dilated. The two parts of the layer interact at the kink, and a density wave forms at the interface due to the large density gradient. The density wave propagates toward the dilated part until the compact part loses contact with the plate. The density wave drives a collisional momentum transfer and pushes the interface toward the dilated part (the kink is shifted rightward at $t=1.2T$ compared to its earlier location at $t=0$). In the next cycle, the same process occurs in the opposite direction, and the kink is pushed back to its original position (not shown in Fig. 10), provided that the phase difference is exactly π (then both parts of a 2D layer are symmetric). As a result, the momentum flux across a kink in a 2D or quasi-2D layer oscillates symmetrically with a

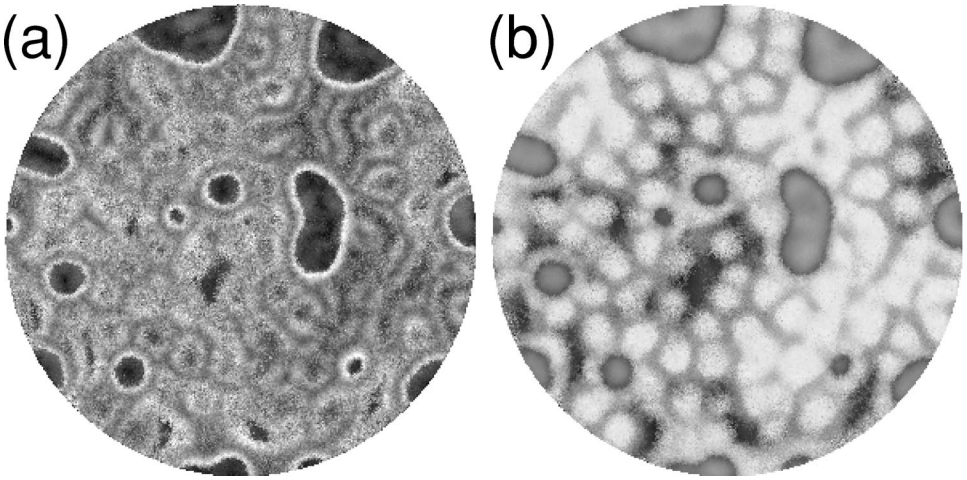

FIG. 9. (a) Horizontal momentum field $\langle \sqrt{p_x^2+p_y^2} \rangle (x,y)$, which has its maximum values (indicated white) along the boundary of phase bubbles; there is a significant momentum flux perpendicular to the boundary (the kink). (b) Vertical momentum field $\langle p_z \rangle (x,y)$, black being the maximum downward, and white being the maximum upward. The fluctuation in vertical momenta (blackish areas) is due to the large scale undulation of the layer, discussed in Sec. IV. These are obtained from the same simulation data as in Fig. 4(d).

period of $2T$, with no net translational motion; thus a phase bubble in a 2D or quasi-2D layer never shrinks but only oscillates symmetrically [Fig. 11(a)].

The mechanism of the density wave and the momentum transfer across a kink in a 3D layer is the same as in a 2D or quasi-2D layer; however, in a 3D layer, there is a geometric effect that is absent in a 2D or quasi-2D layer: the two sides of a kink are not symmetric unless the kink is straight. As the particles at the front of the density wave are nearly static with respect to the plate, the momentum flux is roughly proportional to the number of particles at the front of the density wave and the velocity of the container. For a kink with nonzero local curvature, the number of particles at the front of the density wave for the two successive cycles are different, even if the two sides of the kink are exactly π out of phase. Thus the momentum transfer in one direction is always larger than that of the other. This leads to an asymmetric momentum transfer, or an asymmetric oscillatory motion of a kink. Consequently, the total net momentum flux across the boundary of a phase bubble over a multiple of $2T$ is always inward, because its boundary is a kink of a closed shape. As a result, a phase bubble shrinks and disappears. An asymmetric oscillation of a boundary of a phase bubble is shown in Fig. 11(b). The difference in the numbers of particles at the interface of the density wave for the two consecutive cycles is approximately proportional to the local curvature of the kink. Thus, the speed of a kink is roughly proportional to the local curvature, leading to an effective surface tension.

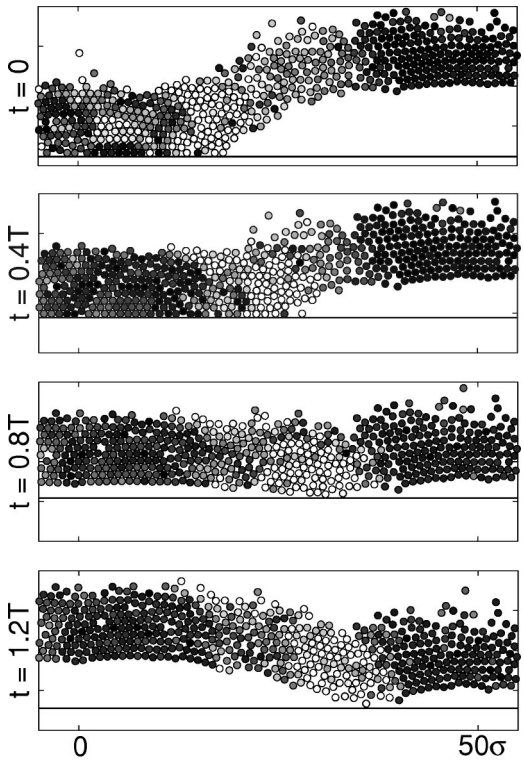

FIG. 10. A sequence of an $f/2$ flat pattern with a kink, obtained from the simulation of a 2D layer for $\Gamma = 5.2$, $f^* = 0.6$, and $N = 9$. Each circle corresponds to a particle. The gray scale of the particles indicates the magnitude of the horizontal momentum $|p_x|$, increasing from black to white. As the layer is pushed up by the plate, a density wave forms, which initiates a momentum transfer propagating rightward (see text for details).

There are other mechanisms driving the motion of a kink in the experiment, which are minor compared to the previously discussed curvature-dependent geometrical effect: (1) *non-π phase difference effect* and (2) *the finite mass ratio effect*. First, we have assumed in the above discussion that both sides of a kink are exactly π out of phase; if this were not the case, the impact from the container for two successive cycles would be different, and the oscillation of a kink would be asymmetric, even if the local curvature were zero. This is why a secondary forcing can control the motion of a straight kink, as was experimentally observed by Aranson *et al.* [19]. Second, if the difference in the mass of each phase domain of the layer is not negligible compared to mass

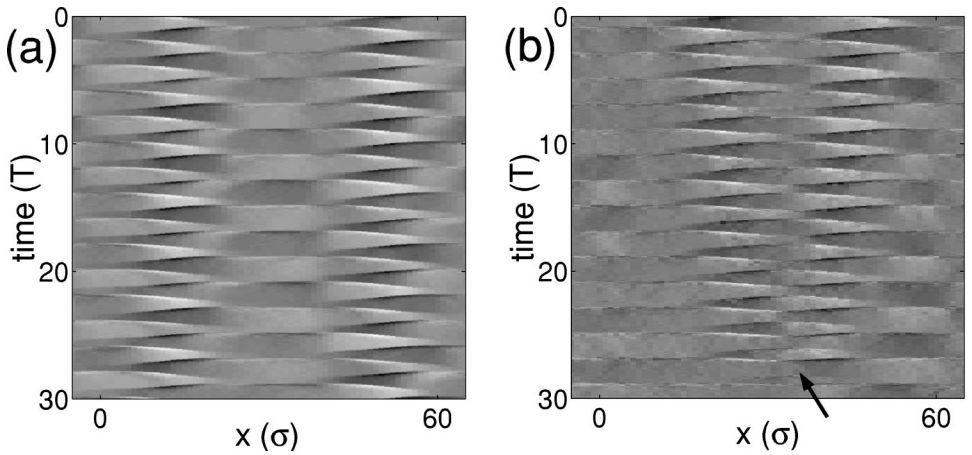

FIG. 11. Space-time plots of horizontal momentum $\langle p_x \rangle(x,t)$ of a phase bubble (a) in a quasi-2D $f/2$ flat pattern, and (b) in a 3D $f/2$ flat pattern (cross section along the diameter of a phase bubble). The values increase from black to white, black being the maximum leftward and white being the maximum rightward. A phase bubble in a quasi-2D layer oscillates symmetrically, while in a 3D layer a bubble oscillates asymmetrically, shrinks and disappears (indicated by an arrow). A quasi-2D layer of size $100\sigma \times 10\sigma$ is used for (a), and the phase bubble in (b) was created by decreasing Γ from 8.5 to 5.2; $f^* = 0.6$ and $N = 6$ for both.

of the container, the impact by the container on both domains of the layer are different, and a net translational motion of a kink is induced, even if it has zero local curvature and the phase difference is π. We call this *the finite mass ratio effect*.

In the experiment, a kink in the $f/2$ flat pattern regime eventually travels to the center of the container, until the impacts from the container on both phase domains are balanced; it was observed in Refs. [16,19]. This effect is absent in the

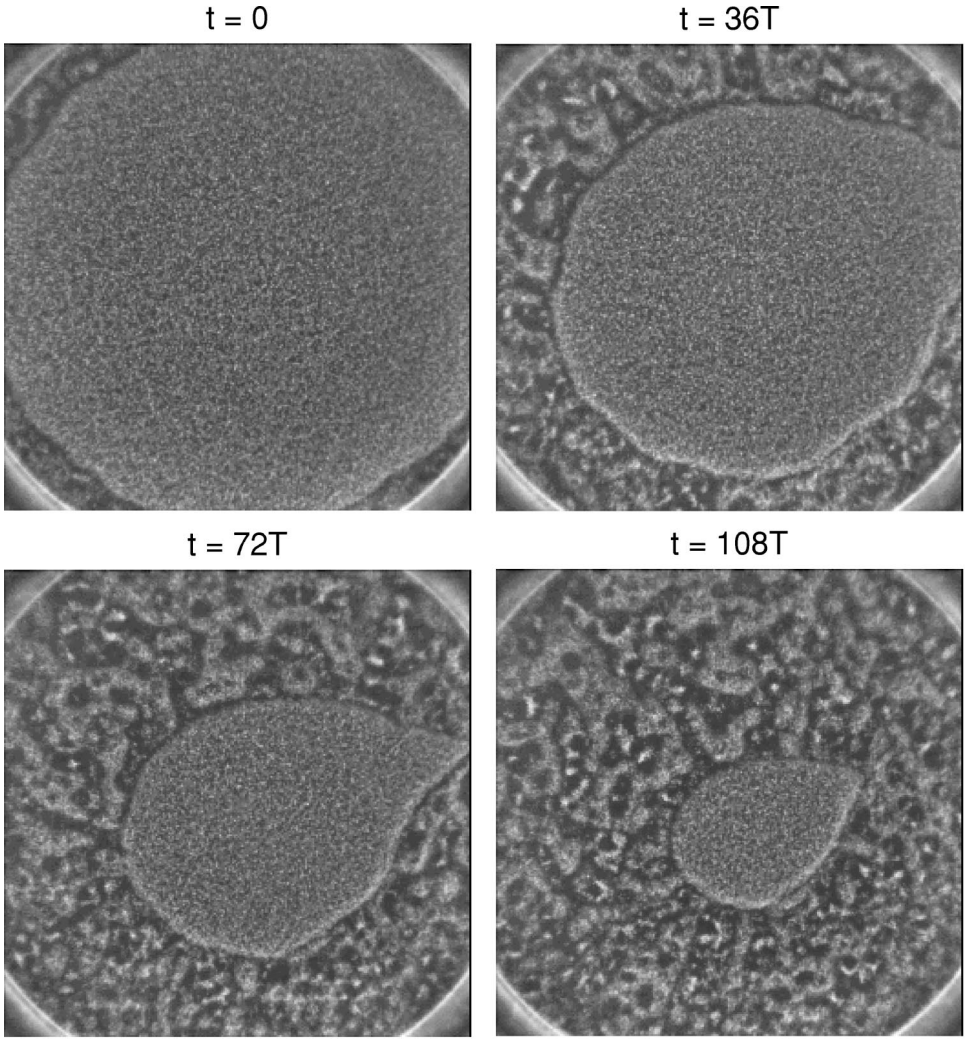

FIG. 12. A sequence of a transient $f/3$ flat pattern obtained from the experiment. The friction due to the side wall creates a kink, which propagates to the center of the container in the radial direction (the same mechanism of the shrinking of a phase bubble) and destroys the $f/3$ flat pattern. Γ was suddenly increased from below the onset, about 2.0 to 7.8; $f^* = 0.94$ and $N = 6$. The experiment was done with the same particles as in Fig. 1, and $L = 847\sigma$.

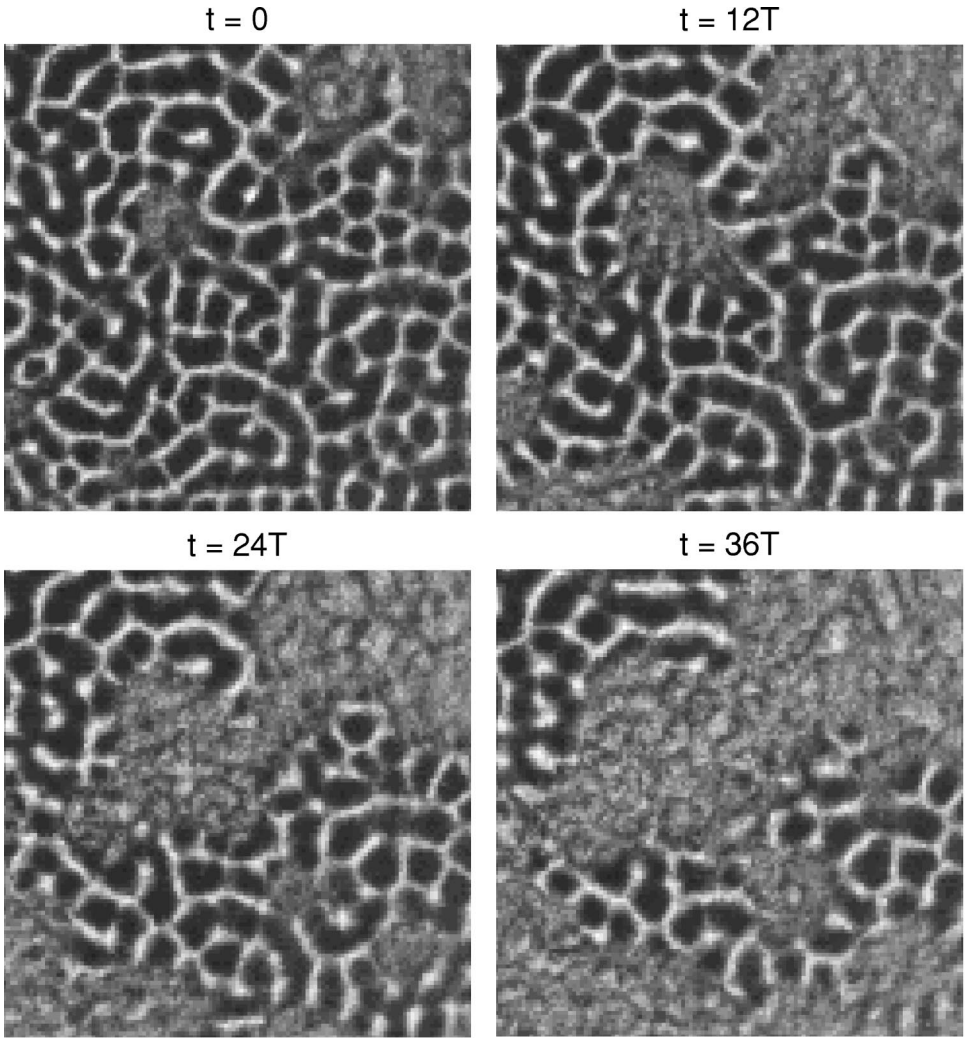

FIG. 13. A sequence of a transient $f/6$ pattern, obtained from the experiment. The undulation of the layer creates kinks in the middle of the layer, which destroys the $f/6$ pattern. Γ was suddenly increased from 2.0 (below pattern onset), to 10 ($f^*=1.2$ and $N=6$). The experiment was done with the same particles, N, and L as in Fig. 13, and a part of the layer of size $250\sigma\times250\sigma$ is shown.

simulation, because the mass of the container is assumed to be infinitely large compared to the mass of the layer.

VI. TRANSIENT *f*/3 AND *f*/6 SUBHARMONIC PATTERNS

Until now, no standing wave pattern has been observed above the $f/4$ hexagonal pattern regime in the phase diagram in Fig. 1. In this section we present the observation of the $f/3$ flat and $f/6$ square-stripe patterns. These patterns were found first in the simulations, which motivated the experiments. We start the discussion with the single ball model.

The single ball model predicts an infinite cascade of bifurcations with increasing natural number n, for increasing Γ (there are small chaotic windows along Γ, but this is not important in this discussion). For the granular layers, these bifurcations correspond to the following patterns:

$$\begin{array}{l} f/n \text{ flat} \leftarrow \\ \quad\downarrow \\ f/(2n) \text{ squares-stripes} \quad n\rightarrow n+1, \\ \quad\downarrow \\ f/(2n) \text{ hexagons} \end{array}$$

where the initial n is 1. This model predicts a bifurcation from an $f/4$ to an $f/3$ state (*Period 1*, $n=3$) at around $\Gamma=8.0$; however, in the experiments, the cascade of bifurcation stops at $n=2$.

We discussed how the undulation of the layer leads to the nucleation of phase bubbles in Sec. IV. If the undulation of the layer could be avoided, we expect that $f/3$ flat and $f/6$ square-stripe patterns would exist. To test this conjecture, we performed a series of numerical simulations of a small layer ($10\sigma\times10\sigma$ and $20\sigma\times20\sigma$ with $N=6$) in the randomly moving labyrinths regime for $(\Gamma,f^*)=(8-11,0.8-1.0)$, using periodic horizontal boundary conditions. In these simulations, we observed that the layer collides with the plate every third cycle, and that the dynamics is stable up to an order of 1000 cycles; we conclude that if a larger layer followed this behavior, $f/3$ or $f/6$ subharmonic patterns would exist.

In larger layers, the undulation of the layer cannot be completely avoided, but can be suppressed at least during a short time by preparing a flat and compact layer as an initial condition; when Γ is quickly increased from the flat pattern regime to where $f/3$ or $f/6$ subharmonic patterns are predicted by the single ball model ($8\lesssim\Gamma\lesssim11$), an $f/3$ or $f/6$

pattern is found in the simulation. Later these transient patterns were found in the laboratory experiments as well, as Figs. 12 and 13 illustrate. These patterns emerge as the primary instability of the layer in this regime, but they are invaded and overtaken by either kinks formed due to the side wall friction (Fig. 12) or by the undulation of the layer (Fig. 13). As a result, the domain of these transient patterns gradually decreases and is eventually taken over by randomly moving labyrinths. These transient patterns last up to several hundreds of cycles, depending on the initial condition, control parameters, and the system size.

VII. DISCUSSION

We have shown that phase bubbles play a critical role in the transition to spatiotemporal chaos in the patterns formed by vertically oscillated granular layers. Phase bubbles spontaneously form first in the $f/4$ hexagonal pattern regime as the acceleration Γ is increased. At larger Γ, the rate of nucleation of bubbles grows faster than the decay rate, leading ultimately to a spatiotemporally chaotic pattern of randomly moving labyrinths. In a qualitatively similar way, the formation of defects has been found to lead to spiral defect chaos [4] and to chaos in a model with invasive defects [12].

We have investigated the mechanism of the nucleation and the dynamics of phase bubbles and randomly moving labyrinths, using inelastic hard sphere molecular dynamics simulations and experiments. We have found that a vertically oscillated granular layer has a large scale undulation, even without interstitial gas (Sec. IV). The undulation constitutes an inherent feature of oscillated granular layers, like the standing wave pattern formation, and cannot be avoided; above some critical value of Γ in the $f/4$ hexagonal pattern regime, the undulation of the layer gives rise to the nucleation of a phase bubble. The spontaneous nucleation of kinks in vertically oscillated 2D or quasi-2D granular layers for large Γ has been called ''subharmonic instability'' [20] or ''arching'' [21,22], but the mechanism has not been elucidated. These two phenomena are all essentially phase bubbles in 2D or quasi-2D oscillated granular layers.

We also found that a kink of nonzero curvature has a net translational motion due to the asymmetric collisional momentum transfer across a kink (Sec. V). The local speed of a kink is roughly proportional to the local curvature; a phase bubble shrinks as if it had a surface tension and then disappears, because it is a kink of a closed form. We showed that shrinking of a phase bubble and translational motion of a kink are essentially the same phenomena.

Finally, based on the understanding of kinks, we predicted transient $f/3$ and $f/6$ subharmonic patterns and observed them (Sec. VI).

ACKNOWLEDGMENTS

The authors thank Professor W. D. McCormick, E. Rericha, B. Lewis, J. Bougie, and N. Peffley for helpful discussions. This work was supported by the Engineering Research Program of the Office of Basic Energy Sciences of the Department of Energy (Grant No. DE-FG03-93ER14312).

[1] M. C. Cross and P. C. Hohenberg, Rev. Mod. Phys. **65**, 851 (1993).
[2] V. Steinberg, E. Moses, and J. Fineberg, Nucl. Phys. B (Proc. Suppl.) **2**, 109 (1987); P. Kolodner, J. A. Glazier, and H. Williams, Phys. Rev. Lett. **65**, 1579 (1990).
[3] A. Pocheau, V. Croquette, and P. Le Gal, Phys. Rev. Lett. **55**, 1094 (1985).
[4] S. W. Morris, E. Bodenschatz, D. S. Cannell, and G. Ahlers, Phys. Rev. Lett. **71**, 2026 (1993).
[5] R. Ribotta and A. Joets, in *Cellular Structures and Instabilities*, edited by J. E. Wesfried and S. Zaslavski (Springer-Verlag, Berlin, 1984); I. Rehberg, S. Rasenat, and V. Steinberg, Phys. Rev. Lett. **62**, 756 (1989).
[6] Q. Ouyang and H. L. Swinney, Chaos **1**, 411 (1991); Q. Ouyang, H. L. Swinney, and G. Li, Phys. Rev. Lett. **84**, 1047 (2000).
[7] A. B. Ezerskiĭ, M. I. Rabinovich, V. P. Reutov, and I. M. Starobinets, Sov. Phys. JETP **64**, 1228 (1986); A. Kudrolli and J. P. Gollub, Physica D **97**, 133 (1996).
[8] C. S. Bretherton and E. A. Spiegel, Phys. Lett. **96A**, 152 (1983).
[9] B. I. Shraiman, Phys. Rev. Lett. **57**, 325 (1986), and references therein.
[10] P. Coullet, L. Gil, and F. Rocca, Opt. Commun. **73**, 403 (1989).
[11] J.-P. Eckmann and I. Procaccia, Phys. Rev. Lett. **66**, 891 (1991).
[12] M. C. Cross and Y. Tu, Phys. Rev. Lett. **75**, 834 (1995); M. Cross, Physica D **97**, 65 (1996).
[13] F. Melo, P. B. Umbanhowar, and H. L. Swinney, Phys. Rev. Lett. **72**, 172 (1994).
[14] C. Bizon, M. D. Shattuck, J. B. Swift, W. D. McCormick, and H. L. Swinney, Phys. Rev. Lett. **80**, 57 (1998).
[15] O. R. Walton, in *Particulate Two-Phase Flow*, edited by M. C. Roco (Butterworth-Heinemann, Boston, 1993), p. 884.
[16] F. Melo, P. B. Umbanhowar, and H. L. Swinney, Phys. Rev. Lett. **75**, 3838 (1995).
[17] Modeling an oscillated granular layer as a perfectly inelastic mass is an old idea. Its dynamics with varying forcing was systematically studied in A. Mehta and J. M. Luck, Phys. Rev. Lett. **65**, 393 (1990).
[18] An animated movie can be found at http://chaos.ph.utexas.edu/research/moon.
[19] I. S. Aranson, D. Blair, W. K. Kwok, G. Karapetrov, U. Welp, G. W. Crabtree, V. M. Vinokur, and L. S. Tsimring, Phys. Rev. Lett. **82**, 731 (1999).
[20] S. Douady, S. Fauve, and C. Laroche, Europhys. Lett. **8**, 621 (1989).
[21] C. R. Wassgren, C. E. Brennen, and M. L. Hunt, Trans. ASME **63**, 712 (1996).
[22] Y. Lan and A. D. Rosato, Phys. Fluids **9**, 3615 (1997).